Engineering properties of sustainable engineered cementitious composites with recycled tyre polymer fibres

Hui Zhong [a], Meng Chen [b], Mingzhong Zhang [a,*]

[a]*Department of Civil, Environmental and Geomatic Engineering, University College London, London WC1E 6BT, United Kingdom*

[b]*School of Resources and Civil Engineering, Northeastern University, Shenyang 110819, China*

Abstract: To lower the material cost and environmental impact of polyvinyl alcohol (PVA) fibre reinforced engineered cementitious composite (ECC), recycled tyre polymer (RTP) fibres were adopted to partially replace PVA fibres in ECC in this study, with an overall aim to develop sustainable ECC with RTP fibres without significantly affecting the engineering properties. A series of tests were conducted to investigate the effect of RTP fibre content on the engineering properties of ECC, with special focus on tensile strain-hardening behaviour and dynamic compressive behaviour. Results indicate that the incorporation of RTP fibres can improve the drying shrinkage resistance of PVA fibre reinforced ECC by 5-13% at 28 d while no positive influences are found on the workability and quasi-static compressive properties. There exists clear strain-hardening behaviour for all studied ECC mixes even when 50% of PVA fibre is substituted with RTP fibre. Based on the results of the micromechanical investigation, all mixtures satisfy the criteria for achieving a robust strain-hardening behaviour. All ECC specimens are characterised by a pronounced strain rate effect under dynamic compression and ECC incorporating RTP fibres shows a stronger sensitivity as opposed to ECC with 2.0% PVA fibre. The material cost and energy consumption of ECC are reduced by about 11-45% and 5-18%, respectively, when RTP fibres are present. This study proves the feasibility of utilising RTP fibres in ECC to improve its sustainability and maintain acceptable static and dynamic mechanical properties while the incorporated fibre volume fraction should be limited to 0.5%.

Keywords: Strain-hardening cementitious composites; Hybrid fibre reinforced concrete; Recycled fibres; Split Hopkinson pressure bar; Mechanical properties; Sustainability

1. Introduction

To overcome the inherent brittleness of ordinary cement-based materials, a special class of high-performance fibre reinforced cementitious composites named engineered cementitious composites (ECC) or strain-hardening cementitious composites were developed [1]. ECC exhibits superior tensile strain-hardening behaviour accompanied by multiple cracks leading to a tensile ductility of at least 2%, several hundred times higher than that of conventional concrete [2, 3]. Besides, the crack width of ECC is typically less than 100 μm under the loading state, which can benefit the durability of concrete structures containing it [1, 4].

* Corresponding author. E-mail address: mingzhong.zhang@ucl.ac.uk (M. Zhang)

Hydrophilic polyvinyl alcohol (PVA) or hydrophobic polyethylene (PE) fibres were usually adopted to manufacture ECC because of their excellent properties [5, 6]. However, the cost and environmental impact of producing these fibres would limit the large-scale application and sustainability of ECC [1, 7, 8]. For instance, a previous study reported that the material cost and embodied energy of ECC containing 2.0% (by volume) PVA fibre were 7.6 and 1.5 times higher compared to those of commercial Grade 45 concrete [9]. To address these issues, a rising number of studies have been focused on developing ECC reinforced with recycled fibres. The existing studies on the effect of recycled polyethylene terephthalate (PET) fibre on the engineering properties of ECC indicated that the uniaxial tensile behaviour of ECC was weakened when PVA fibres were partially replaced with recycled PET fibres [9-11]. For instance, employing 1.0% recycled PET fibre without any pre-treatment to replace PVA fibre reduced the tensile strength and tensile strain capacity of ECC with 2.0% PVA fibre by 30.56% and 60.48%, respectively [9]. Nevertheless, the material cost and environmental impact of ECC were reduced significantly in the presence of recycled PET fibres. In addition, ECC containing 1.0% PVA fibre and 1.0% recycled PET fibre had comparable impact behaviour to ECC with 2.0% PVA fibre along with acceptable uniaxial tensile behaviour [11].

Given that a significant amount of scrap tyres is produced every year (about 26 million tonnes [12]), crumb rubber recycled from end-of-life tyres was used to partially or fully replace silica sand in ECC for improving its sustainability. It was reported that the tensile strain capacity of ECC can be improved in the presence of crumb rubber due to the reduced matrix toughness and chemical bonding between fibre and matrix [13-17]. Besides, the incorporation of crumb rubber into ECC can increase the number of active flaws, which is beneficial for tensile ductility [1, 5]. For instance, using 20% (by volume) crumb rubber to replace silica sand in ECC led to a 51.86% enhancement in tensile strain capacity [16]. Nevertheless, the presence of crumb rubber weakened the strength and drying shrinkage resistance due to its low stiffness and poor bonding with matrix [5]. A few studies found that crumb rubber has a great potential to improve the impact performance of ECC [15, 18]. Except for crumb rubber, the tyre recycling plant can also produce recycled fibres, e.g., recycled tyre polymer (RTP) fibres [19]. Finding a suitable usage for these fibres is essential as accumulating them may result in many environmental problems [20]. Using an appropriate RTP fibre dosage in concrete can improve its resistance against high temperature or fire exposure [21, 22], shrinkage [23, 24], freeze-thaw cycles [20, 25], and dynamic and fatigue loadings [26-29], suggesting the potential of adopting RTP fibres in ECC to improve certain properties while reducing the material cost and environmental impact. Apart from the static mechanical properties, the dynamic mechanical properties of ECC have been increasingly studied as concrete structures would experience both static and dynamic loadings during their service life. The ductility and energy absorption capacity of ECC were greater than those of plain mortar under dynamic compressive loading, making it suitable for preventing structural

members from failure under various impact loadings [30]. ECC outperformed conventional concrete in terms of dynamic fracture energy, about 50 times higher [31]. Besides, there existed a more pronounced strain rate effect in dynamic tensile strength as compared with high-strength concrete and ultra-high performance concrete because of the improved fibre bridging effect as a result of better fibre properties and fibre-matrix bonding [31, 32]. Owing to the excellent energy absorption capacity under uniaxial tension, ECC exhibited the smallest crater volume under high velocity projectile impact loading in comparison with ultra-high performance fibre reinforced concrete and high-strength fibre reinforced concrete [33]. Similarly, it was found that the superior ductility of ECC can improve the resistance of structural elements against impact loading by allowing the steel reinforcement to undergo plastic yielding [34]. These findings suggest that ECC has a great potential for applications against dynamic loadings (e.g., military construction and aeroplane runways) compared to ordinary concrete and other high-performance concrete. To assess the feasibility of using RTP fibres to develop a sustainable ECC for widespread applications, it is of great importance to evaluate the effect of RTP fibre content on both static and dynamic properties of ECC, which has not been explored yet.

This study aims to comprehensively investigate the effect of partial substitution of PVA fibres with RTP fibres (0.25-1.0%, by volume) on the engineering properties of ECC, focusing on the uniaxial tensile and dynamic compressive performance. Different tests were conducted to measure the workability, compressive strength, elastic modulus, and uniaxial tensile and dynamic compressive properties of studied ECC mixes. Both micromechanical and microstructural investigations were carried out to understand the uniaxial tensile behaviour of ECC. A 100-mm diameter split Hopkinson pressure bar (SHPB) apparatus was employed to characterise the dynamic compressive behaviour of ECC in terms of failure pattern, dynamic compressive strength, dynamic increase factor (DIF), and energy absorption capacity.

2. Experimental program

2.1. Raw materials

The materials used in this study to prepare ECC specimens consist of P.I. 42.5R Portland cement conforming to the Chinese standard GB/T 175-2007 [35], low-calcium fly ash as per ASTM C618-17a [36], silica sand, polycarboxylate-based superplasticiser, and oil-coated PVA fibres (Kuraray Co., Ltd., Japan) and RTP fibres recycled from end-of-life tyres. Table 1 gives the chemical compositions of cement and fly ash, while Fig. 1 presents the particle size distribution of cement, fly ash and silica sand. The properties of fibres adopted are listed in Table 2, where the properties of PVA fibres were supplied by the producer while those of RTP fibres were characterised by the authors, as illustrated in detail in previous studies [29, 37]. It should be mentioned that a cleaning process was performed

on all RTP fibres to eliminate the attached rubber particles and impurities [26, 37]. Fig. 2 illustrates the photos and microscopic images of RTP fibres following the cleaning process.

Table 1 Chemical compositions (wt.%) of ordinary Portland cement and fly ash.

Oxide	SiO_2	Al_2O_3	CaO	Fe_2O_3	SO_3	MgO	TiO_2	P_2O_5	Loss on Ignition
Cement	19.39	4.34	68.07	3.14	2.40	1.37	0.21	0.10	2.40
Fly ash	57.02	32.35	2.88	3.01	0.41	0.58	1.26	0.20	2.45

Table 2 Properties of fibres adopted in this study.

Fibre	Length (mm)	Diameter (μm)	Tensile strength (MPa)	Elastic modulus (Ga)	Density (kg/m^3)	Melting temperature (°C)
PVA	12	40	1560	41	1300	248
RTP	5.2 (2.4)[a]	21.4 (4.4)[a]	761 (115)[a]	3.8 (0.7)[a]	1476 (3)[a]	254

Note: [a] standard deviation.

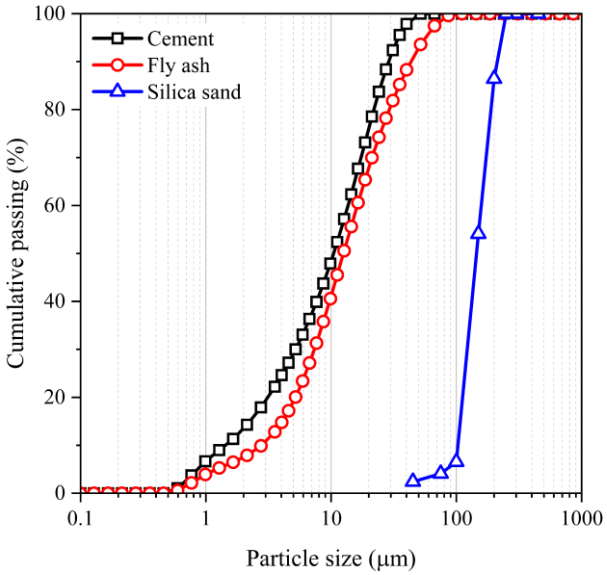

Fig. 1. Particle size distribution of cement, fly ash and silica sand.

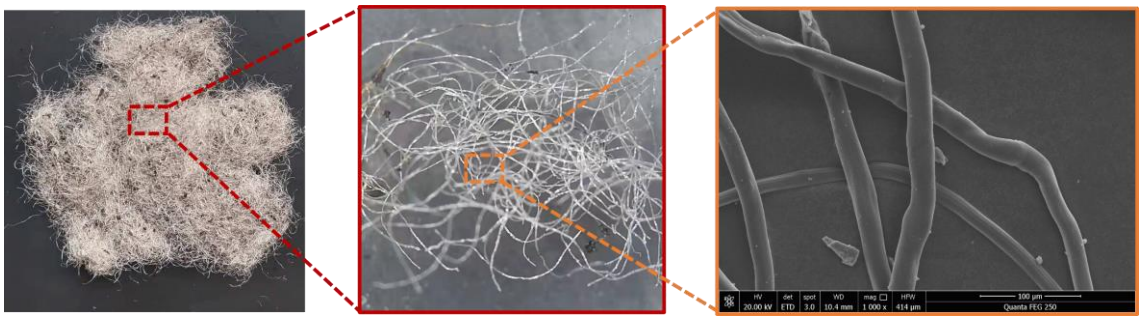

Fig. 2. Physical appearance of RTP fibres.

2.2. Mix proportions

Table 3 presents the mix proportions adopted in this work. A constant water-to-binder ratio of 0.27 was applied. The mass ratio of cement, fly ash and silica sand was 1:1.2:0.8 and the content of superplasticiser was selected as 0.4% of binders weight. In terms of the mix ID displayed in Table 3, 'P2' represents the mixture reinforced with 2.0% PVA fibre, while 'P1R1' denotes the mixture

containing 1.0% PVA fibre and 1.0% RTP fibre. A previous study [9] indicated that ECC with less than 1.0% PVA fibres did not exhibit a conspicuous strain-hardening behaviour. Additionally, the mechanical properties of cementitious composites were impaired substantially when the volume fraction of incorporated RTP fibre reached near 1.0% [27]. To ensure the unique tensile strain-hardening behaviour and acceptable mechanical properties for all investigated ECC mixtures containing RTP fibres, the highest fibre replacement ratio was thus set as 1.0% here.

2.3. Sample preparation

All fresh mixtures were produced at room temperature. For P2, the following mixing procedure was used: (1) mix cement, fly ash and silica sand for 2 min to achieve homogeneous dispersion; (2) add water and mix for 5 min; (3) add superplasticiser and mix for 4 min; and (4) PVA fibres were slowly added to ensure the even fibre dispersion. Regarding specimens containing both PVA and RTP fibres, RTP fibres were first mixed with a certain content of total mixing water and added after the first step mentioned above to avoid uneven dispersion of them [23, 38]. The total mixing time for all mixtures was around 15 min. All specimens were de-moulded after 24 h of curing at 20 ± 2 °C and then moved into a standard moist curing room (20 ± 2 °C, 95% relative humidity) until 28 d (excluding samples for drying shrinkage test). For each test performed in this study, three samples for each mixture were prepared to obtain the average value and standard deviation.

Table 3 Mix proportions of ECC.

Mix ID	By weight (kg/m^3)					By volume (%)	
	Cement	Fly ash	Silica sand	Water	Superplasticiser	PVA fibre	RTP fibre
P2	563	676	451	335	4.96	2.0	0
P1.75R0.25						1.75	0.25
P1.5R0.5						1.5	0.5
P1.25R0.75						1.25	0.75
P1R1						1.0	1.0

2.4. Testing methods

2.4.1. Flow table test

The flow table test was performed on all fresh ECC samples to determine the workability in accordance with ASTM C1437-15 [39].

2.4.2. Drying shrinkage test

As per ASTM C490-17 [40], the drying shrinkage of ECC specimens was attained by measuring the length difference of prismatic specimens with dimension of 25 mm × 25 mm × 280 mm between the day of demoulding and subsequent days cured in a room with 20 ± 2 °C and relative humidity of 50% ± 5%.

2.4.3. Quasi-static mechanical tests

Quasi-static compression tests were conducted on ECC specimens with two different sizes (50 mm cubic [41] and Ø 100 mm × 200 mm cylindrical samples [42]). The adopted loading rate was 1.0 mm/min. Before the test, the end surfaces of all cylindrical samples were treated to guarantee their flatness. The measured quasi-static compressive strength based on the cylindrical sample was selected to calculate the DIF to reduce the specimen size and end friction effects [43, 44].

The elastic modulus of all studied mixtures was measured based on the slope of the compressive stress-strain curve (up to 40% of the ultimate load-carrying capacity) [45]. The used sample size was Ø 100 mm × 200 mm and two strain gauges were installed at the mid-height of the tested sample to obtain the longitudinal strain.

Uniaxial tension tests were carried out on ECC specimens with dog-bone shapes adopting a constant loading rate of 0.5 mm/min [46]. Fig. 3 displays the testing configuration and the size of the employed specimen whilst the test. Two linear variable displacement transducers (LVDTs) were used to record the deformation of the gauge part with a length of 80 mm. In addition, the cracking pattern within this gauge region was photographed and analysed.

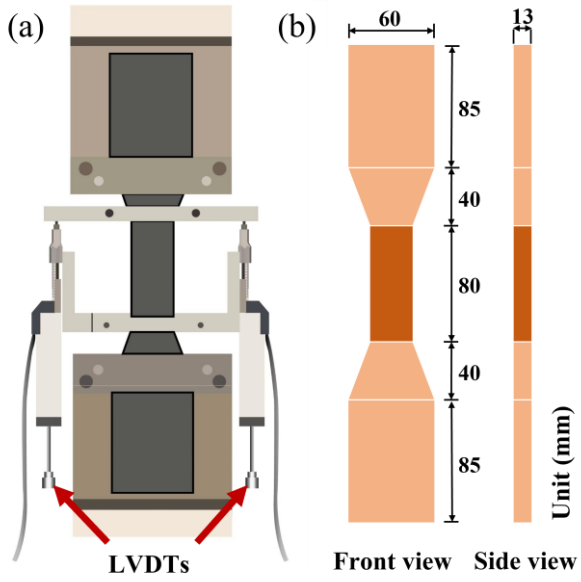

Fig. 3. Schematic diagram of (a) testing setup and (b) dog-bone shaped specimen for uniaxial tensile test.

The unique tensile behaviour of ECC can be achieved using the micromechanics-based theory, where two criteria (strength-based and energy-based) must be satisfied to ensure it [1]. The strength-based criterion shown below is to guarantee the cracking strength would not exceed the fibre bridging stress:

$$\sigma_{fc}, \sigma_c < \sigma_0 \quad (1)$$

where σ_{fc} represents the stress needed to generate the first crack, σ_c is the stress needed to form another crack (multiple cracks are generated already), and σ_0 denotes the maximum fibre bridging stress.

The energy-based criterion is to ensure a steady-state crack propagation mode for ECC after the appearance of the first crack, where the maximum complementary energy (J'_b) for fibre bridging must be greater than the energy consumed by fracturing the matrix (J_{tip}):

$$\begin{cases} J'_b \geq J_{tip} = K_m^2/E_m \\ \sigma_0\delta_0 - \int_0^{\delta_0} \sigma(\delta)\, d\delta = J'_b \end{cases} \tag{2}$$

where δ_0 and δ_{ss} denote the crack openings corresponding to σ_0 and σ_{ss}, respectively, and K_m and E_m are the fracture toughness and elastic modulus of the matrix, respectively.

To verify whether the investigated ECC mixes can satisfy the above criteria, it is vital to obtain the relation between tensile stress and crack opening shown in Fig. 4. To attain it, single crack direct tension tests were performed on notched dog-bone shaped specimens (Fig. 5) [47]. Two LVDTs were used to measure the opening of the crack [48, 49]. The loading rate was consistent with that adopted during the uniaxial tensile test.

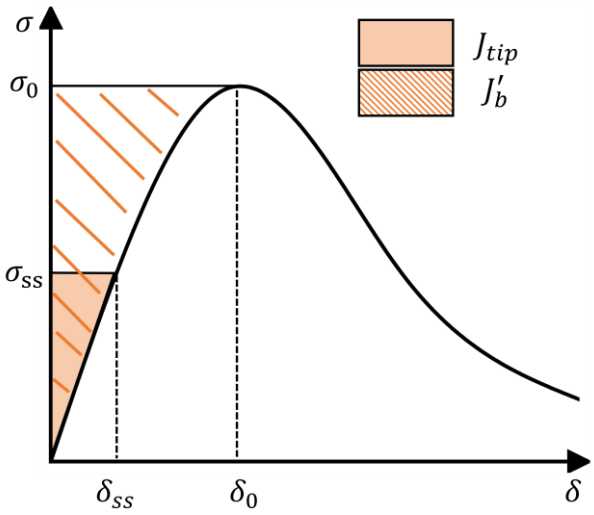

Fig. 4. Typical fibre bridging stress-crack opening response [1].

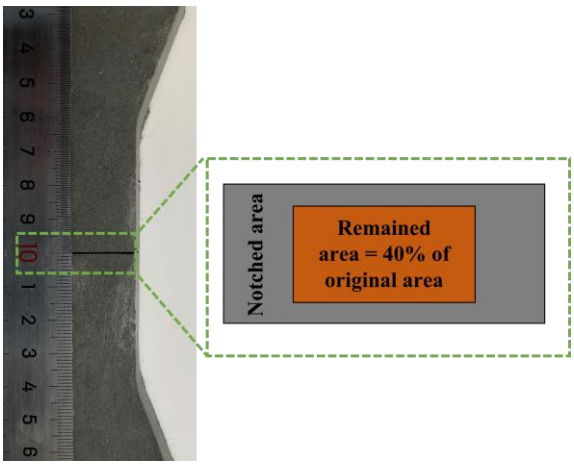

Fig. 5. Notched dog-bone shaped specimen for single crack direct tension test.

According to RILEM FMC-50 [50], three-point bending tests were carried out on notched prismatic samples with sizes of 40 mm × 40 mm × 160 mm (without fibres) to achieve K_m that is an important parameter of calculating J_{tip} (see Eq. (2)).

2.4.4. Dynamic compressive test

A 100-mm diameter SHPB testing device was employed to characterise the dynamic compressive behaviour of ECC mixes, the schematic illustration of which is given in Fig. 6. Prior to the test, the sample with a size of ∅ 100 mm × 50 mm was sandwiched between the incident and transmission bar and adopting this sample size was to reduce the inertia effect during the dynamic compression [27, 51]. The loading ends of the test specimens must be flat and were covered by some grease to lower the influence of end friction [52]. After the test started, the incident ($\varepsilon_i(t)$), reflected ($\varepsilon_r(t)$) and transmission ($\varepsilon_t(t)$) pulses were generated and then collected by the strain gauges mounted on the incident and transmission bars. The history of dynamic compressive stress ($\sigma(t)$), strain ($\varepsilon(t)$) and strain rate ($\dot{\varepsilon}(t)$) can be determined based on these collected strain values as follows [53]:

$$\begin{cases} \sigma(t) = \dfrac{E_1 A_1}{2A_2}(\varepsilon_i(t) + \varepsilon_r(t) + \varepsilon_t(t)) \\ \varepsilon(t) = \dfrac{C_b}{l_2}\displaystyle\int_0^t (\varepsilon_i(t) - \varepsilon_r(t) - \varepsilon_t(t))\ dt \\ \dot{\varepsilon}(t) = \dfrac{C_b}{l_2}(\varepsilon_i(t) - \varepsilon_r(t) - \varepsilon_t(t)) \end{cases} \quad (3)$$

where E_1, A_1 and C_b represent the elastic modulus, cross-sectional area and wave propagation velocity of the bar, respectively, and A_2 and l_2 stand for the cross-sectional area and length of the ECC specimen, respectively.

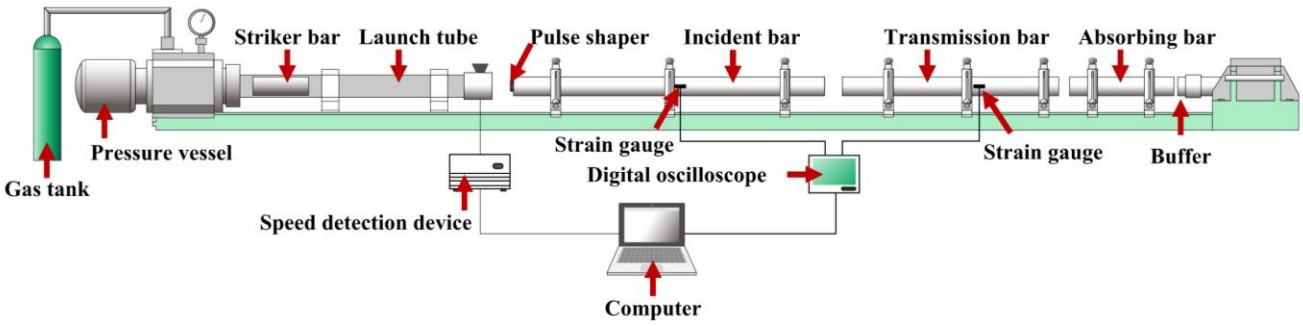

Fig. 6. Schematic illustration of SHPB device for dynamic compressive test.

3. Results and discussion

3.1. Workability

Fig. 7 shows the slump flow of all mixtures, ranging from 191.5 mm to 198.8 mm. In general, the inclusion of RTP fibres did not significantly vary the workability of ECC although a downward trend was observed. The slump flow of P1R1 was 3.69% lower than that of P2. The influence of hybrid

fibres on the workability would be different from that of mono-fibre, where the mutual effect between different incorporated fibres could restrict each other's rotation and thereby affect the fibre orientation to the flow direction of mortar/paste [54]. It should be noted that the flowability tends to be further reduced when more fibres align perpendicular to the flow direction of mortar/paste. A congested fibre network could be formed if more RTP fibres with ununiform dimensions are combined with stiffer PVA fibres [37, 55], leading to reduced workability for ECC.

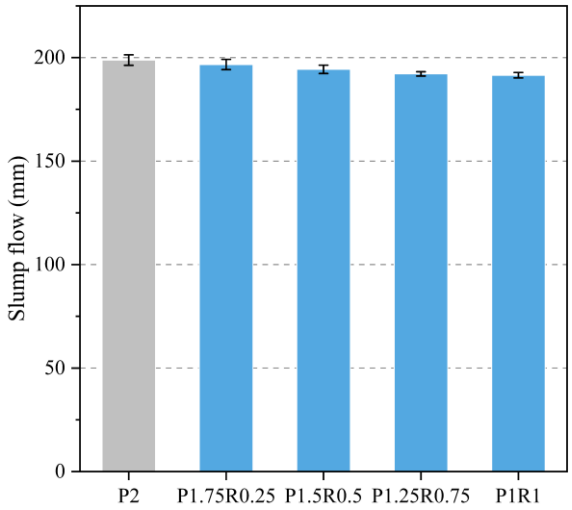

Fig. 7. Effect of RTP fibre content on slump flow of ECC.

3.2. Drying shrinkage

The volume stability of ECC mixes can be reflected by their drying shrinkage, the results of which are displayed in Fig. 8. The 28-d drying shrinkage of all ECC specimens ranged from 1353 με to 1557 με, which was larger than that of traditional ECC reported in Ref. [56] (1200 με) because of the lower water-to-binder ratio adopted in this study. Similar to other ECC [56, 57], all mixtures here had a rapid increase of drying shrinkage up to about 11 d and after which, the rise of drying shrinkage tended to be stabilised. A positive influence of RTP fibre on the drying shrinkage resistance was captured. For instance, the 28-d drying shrinkage of hybrid fibre reinforced ECC was about 5-13% lower in comparison with P2. Such positive effect of RTP fibre in resisting shrinkage of cement-based and geopolymer composites was also observed by other studies [20, 23, 24, 37], which can be ascribed to the hydrophobic feature of RTP fibre that can gradually release some blocked liquid during the drying. Although most of the rubber particles attached to RTP fibres were removed after the cleaning process, some tiny rubber particles may still exist which can store some water during the mixing and gradually release as time goes by [26, 58]. The synergistic effect of hybrid fibres in limiting the shrinkage-induced cracks at different scales also contributed to the reduction of drying shrinkage. RTP fibres are effective in preventing the micro-cracks induced by drying shrinkage from growing and propagating, while PVA fibres can fully utilise their restraining function when facing shrinkage cracks with larger sizes.

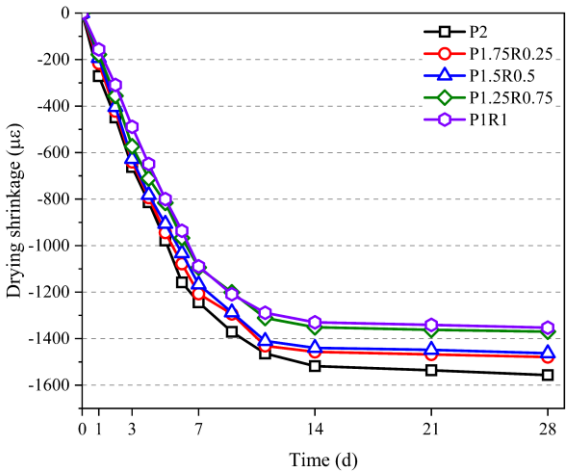

Fig. 8. Effect of RTP fibre dosage on drying shrinkage of ECC.

3.3. Quasi-static compressive strength

Fig. 9 illustrates the effects of RTP fibre dosage and specimen size on the quasi-static compressive strength of ECC. Regardless of test specimen size, P2 achieved the highest compressive strength at 28 d, approximately 7-40% higher than that of ECC with hybrid fibres. The decreased compressive strength of ECC induced by the presence of RTP fibres can be associated with the following reasons: (1) the reduced crack-controlling ability as a result of weaker bonding between RTP fibre and matrix, shorter length and lower strength of RTP fibre [37]; and (2) the existence of some tiny rubber granules that can further weaken the fibre-matrix bonding [59]. Similar findings were observed in previous studies that increasing the RTP fibre content can lower the compressive strength of concrete/mortar [23, 27].

The compressive strength of cement-based materials can be affected by several factors such as specimen size and boundary condition [55]. The commonly used specimen size of ECC for the quasi-static compression test is a 50 mm cube [41], which is considerably smaller than that of most structural elements. For practical applications, it is crucial to evaluate the size effect on the quasi-static compressive strength of ECC. Irrespective of reinforcing fibre, the compressive strength of cylindrical ECC specimens was 0.52-12.85% smaller than that of cubic samples. The induced disparate compressive strengths for specimens with different sizes are due to the friction at the contact region between specimen and loading plate, where the lateral expansion of the test specimen is limited offering transversal compressive stress on it [60]. Hence, the specimen with a large contact area with the loading plate should present a higher compressive strength. However, this statement is not valid for the results here, which can be associated with their different fracturing processes. The aspect ratio of the cylindrical sample (2.0) was larger than that of the cubic sample (1.0) here, which may have a larger mid-portion area experiencing pure tension [43]. Therefore, when the number of effective fibres within this pure tension region reduces, the compressive strength would be much lower. This

can explain why the difference between cubic and cylindrical compressive strengths for hybrid fibre reinforced ECC went up with the rising RTP fibre content.

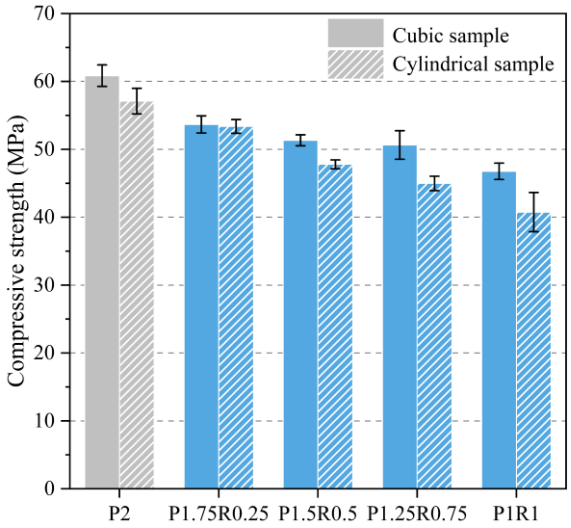

Fig. 9. Effects of specimen size and RTP fibre content on compressive strength of ECC.

3.4. Elastic modulus

Fig. 10a depicts the elastic modulus of all ECC specimens, revealing that the trend of elastic modulus with RTP fibre replacement dosage was consistent with that of quasi-static compressive strength. The elastic modulus of ECC containing RTP fibres was 1.50-14.65% lower than that of mono-PVA fibre reinforced ECC mainly due to the poorer internal structure along with higher porosity. The lower elastic modulus of RTP fibre may also partly contribute to the decreased elastic modulus of overall composites. This finding shows a good agreement with previous studies regarding the effect of RTP fibre on the elastic modulus of concrete [20, 28].

Fig. 10b compares the current results of elastic modulus with the existing equations for predicting the elastic modulus of ordinary concrete [61, 62] and the results of elastic modulus acquired from other studies on ECC [63-65]. Similar to the trends of two predicting equations, a positive correlation can be found between elastic modulus and compressive strength for all ECC mixtures. However, the equations for Portland cement concrete overestimated the elastic modulus of ECC, which can be primarily assigned to the elimination of coarse aggregate and the addition of flexible fibre into ECC mixtures. It was found that regardless of reinforcing fibre, the elastic modulus of ECC went up with the increase of sand-to-binder ratio [65]. Although steel fibres (210 GPa) have a higher elastic modulus than PE fibres (100 GPa), replacing 1.0% PE fibre with steel fibre reduced the elastic modulus of mono-PE fibre reinforced ECC by around 9% due to the introduction of more defects by steel fibres [65]. This supports the previous discussion that the quality of internal structure plays a more important role in the elastic behaviour of ECC. Similarly, due to the increased porosity, the presence of rubber granules weakened the elastic modulus of ECC [64], suggesting that the existence of small rubber particles on the surfaces of adopted RTP fibres in this study may partially contribute

to the drop in elastic modulus. Based on the data shown in Fig. 10b, a new model with R^2= 0.956 can be proposed to describe the relationship between elastic modulus (E_c) and compressive strength (f_c) of ECC:

$$E_c = 0.874 f_c^{0.809} \quad (4)$$

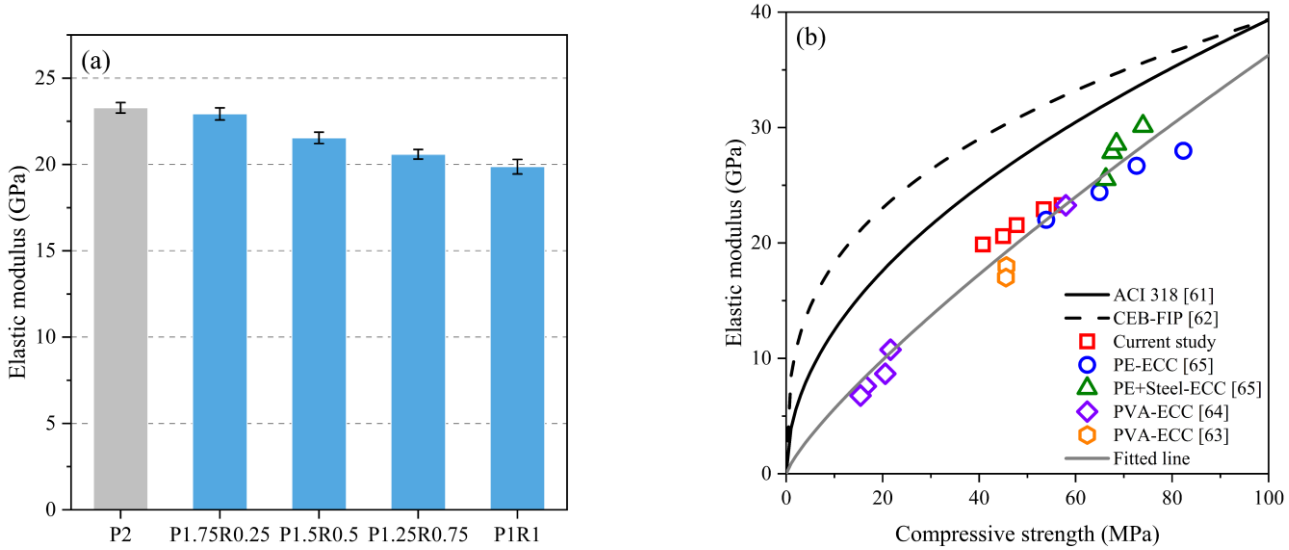

Fig. 10. Elastic modulus of ECC: (a) with various RTP contents, and (b) in relation to compressive strength.

3.5. Uniaxial tensile behaviour

3.5.1. Stress-strain response

The tensile stress-strain response of ECC is presented in Fig. 11, which can be mainly divided into two pronounced parts, including linear elasticity and strain-hardening regions. The tensile stress corresponding to the end of the linearity region is called first cracking strength, while the highest point of tensile stress is uniaxial tensile strength and the strain at that point is defined as tensile strain capacity. After the appearance of the first visible crack, all ECC samples strain-hardened until the ultimate failure, while the strain-hardening region of ECC was shortened when PVA fibres were substituted with RTP fibres. The tensile stress-strain response of all mixes was consistent with their final cracking patterns shown in Fig. 12, where the number of induced cracks declined with the rising RTP fibre content. To further evaluate the RTP fibre effect on the uniaxial tensile performance of ECC, some typical tensile properties derived from the stress-strain curves (i.e., first cracking strength, tensile strength, tensile strain capacity, and tensile strain energy) are discussed comprehensively in the next section.

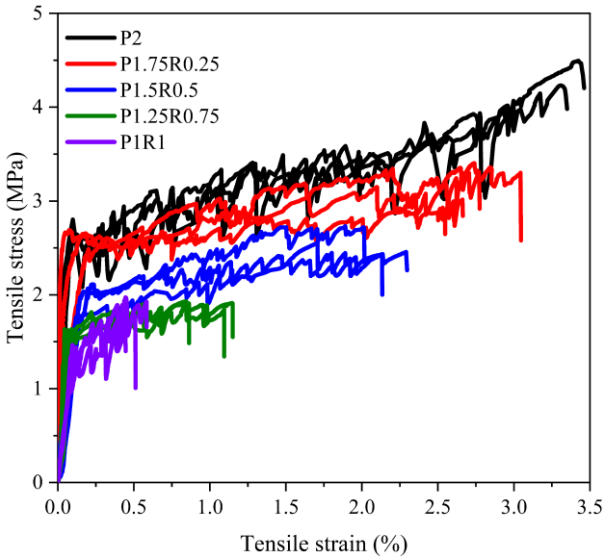

Fig. 11. Tensile stress-strain curves of all ECC mixtures.

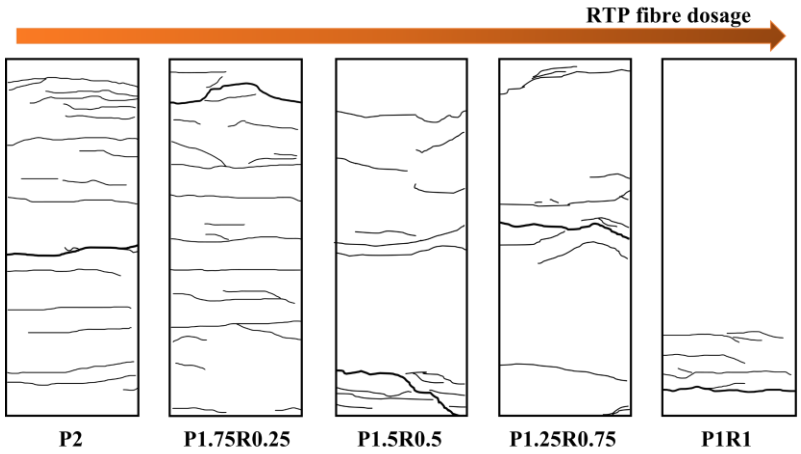

Fig. 12. Cracking patterns of all ECC mixtures.

3.5.2. Tensile properties

Fig. 13 summarises the typical tensile properties of all ECC specimens. The first cracking strength relies on K_m and internal pore size as well as the fibre bridging behaviour if the internal pore is bridged by the fibres [1]. As seen in Fig. 13a, P2 attained the highest first cracking strength of 2.7 MPa, while that of hybrid fibre reinforced ECC was 6.30-47.41% lower as compared with P2. Since all ECC studied here shared the same matrix, K_m was not the dominant factor influencing the first cracking strength. When more PVA fibres were present, the first cracking strength of the whole composite tended to be higher, which can be ascribed to the effective fibre bridging action of PVA fibres [66, 67]. Similar findings were captured by other studies [37, 67, 68].

The tensile strength and strain capacity of ECC displayed in Figs. 13b and c were consistent with the first cracking strength. More specifically, the tensile strength and tensile strain capacity of ECC containing RTP fibres were 23.76-56.24% and 15.79-85.45% lower, respectively, in comparison with P2. When 50% of PVA fibre was replaced with RTP fibre, the tensile strain capacity of the resultant composite was only 0.47%, which can be ascribed to similar reasons explained for quasi-static

compressive strength (Section 3.3). Fibre distribution also can considerably affect the tensile properties of ECC. If the cracking plane has more RTP fibres instead of PVA fibres, the localisation of fracture would happen, and no more new cracks can be induced because of the insufficient bridging stress to restrain the crack opening. Previous studies reported similar findings when recycled PET fibres [9, 10] or polypropylene fibres [69] were employed to partially replace PVA fibres in ECC. Fig. 13d presents the tensile strain energy of ECC which was calculated by integrating the rising region of the tensile stress-strain curve (Fig. 11). Similar to other tensile properties, the inclusion of RTP fibres did not benefit the tensile strain energy of ECC and P2 attained the largest value of 104.28 kJ/m^3.

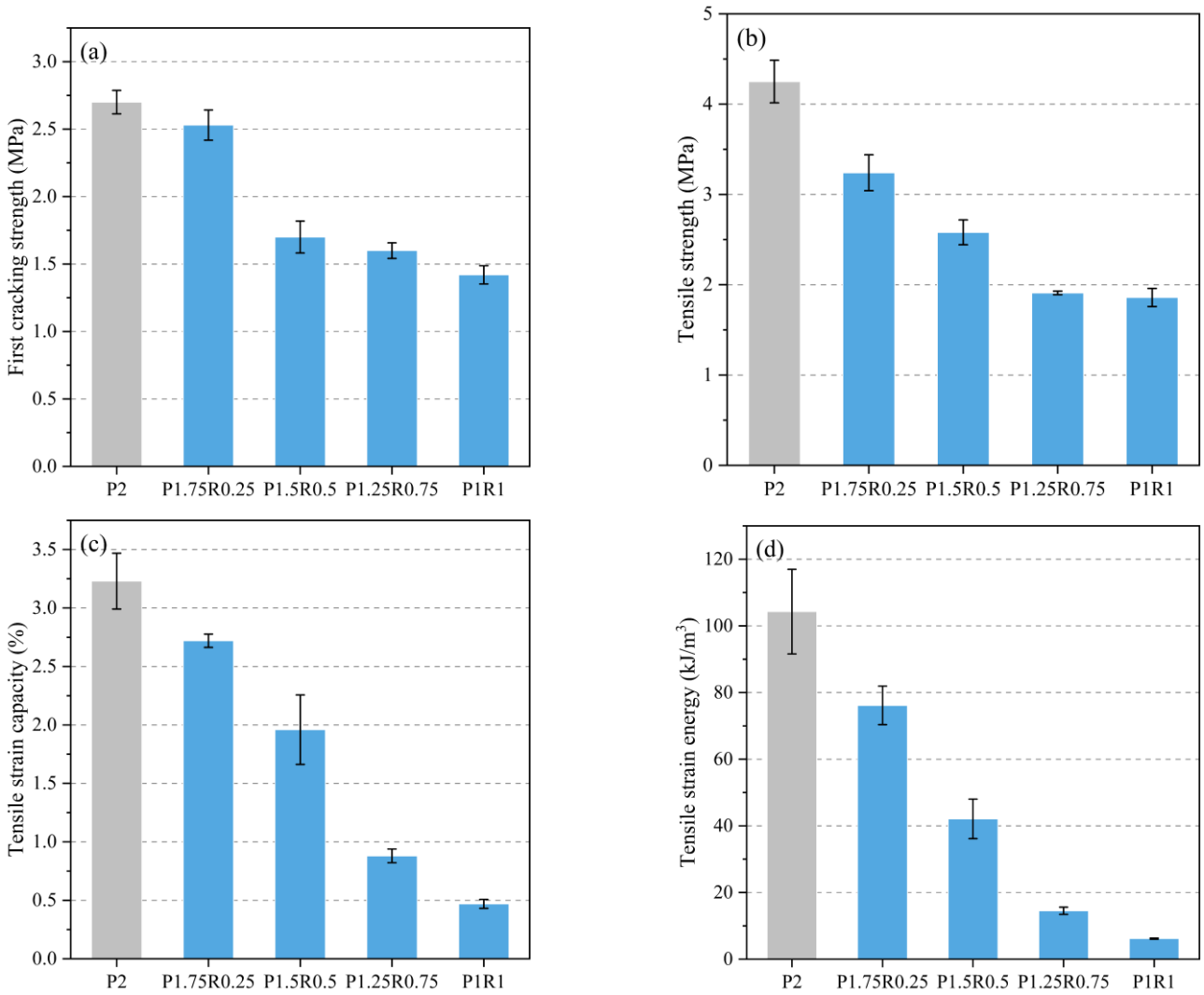

Fig. 13. Tensile properties of ECC specimens: (a) first cracking strength, (b) tensile strength, (c) tensile strain capacity, and (d) tensile strain energy.

To better interpret the tensile behaviour of investigated ECC mixes, the fibre statuses at the cracking interfaces were investigated using scanning electron microscopy (SEM) and the microscopic images are presented in Fig. 14. Because of the strong frictional bonding with the matrix, conspicuous abrasion traces were found on the surfaces of PVA fibres. Both pulled out and ruptured PVA fibres

can be observed and the former one was more beneficial to the tensile properties of ECC relative to the latter one. PVA fibre rupture can considerably limit the tensile strain capacity of ECC, which can happen due to the superior interfacial properties and large inclination angles of fibres [1]. When the PVA fibre with a large inclination angle is present at the cracking interface, its in-situ strength would be reduced significantly caused by local bending stress, lateral stress and fibre surface abrasion [70]. In addition, matrix spalling would happen to reduce the pull-out resistance. By contrast, RTP fibre did not experience a strong frictional pull-out as its surface was much smoother relative to PVA fibre. Hence, the overall tensile properties of ECC were impaired in the presence of RTP fibres. Based on the above results, the RTP fibre replacement dosage should be limited to 0.5% as P1.5R0.5 can still exhibit acceptable tensile properties, especially around 2% for tensile strain capacity.

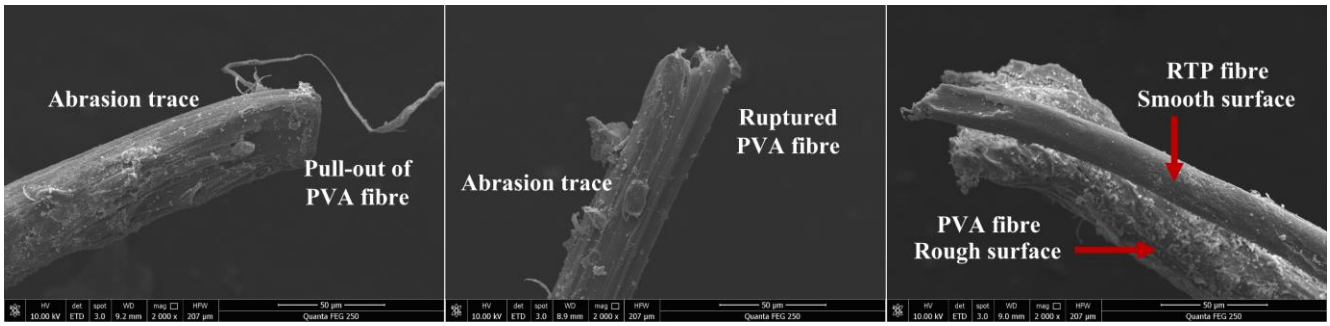

Fig. 14. SEM micrographs of fibre conditions after uniaxial direct tension.

3.5.3. Strain-hardening indices

Table 4 lists the results of single crack direct tension tests and the calculated strain-hardening indices. The maximum fibre bridging stress can be affected by various factors, including fibre dosage, fibre strength and length, and fibre-matrix interfacial properties (especially frictional bond) [1], and can be considered as the stress needed to overcome the bond and pull out the bridging fibres. After exceeding it, the fibres can no longer bridge the crack and are either pulled out completely or ruptured. Utilising RTP fibres to replace PVA fibres impaired both fibre bridging stress and corresponding crack opening mainly due to the poorer interfacial bonding behaviour of RTP fibres, showing a good agreement with the uniaxial tensile properties.

As mentioned in Section 2.4.3, both strength-based and energy-based indices were used to validate the strain-hardening behaviour of ECC. The higher these indices, the larger probability for a specimen to possess saturated and stable strain-hardening and multiple cracking behaviour [71]. Based on Refs. [71, 72], the strength-based index and energy-based index of ECC should be greater than or equal to 1.2 and 2.7, respectively, for attaining a robust strain-hardening behaviour accompanied by a stable multiple cracking feature. The measured K_m, σ_{fc} and J_{tip} were 0.816 MPa·m$^{1/2}$,1.72 MPa and 27.93 J/m^2, respectively. As seen in Table 4, all mixtures fulfilled the above requirements and P2 had the highest values in both indices. A positive correlation was found between these indices and uniaxial tensile properties of ECC.

Table 4 Results of single crack direct tension test and strain-hardening indices.

Mix ID	Results of single crack direct tension test		Strain-hardening indices	
	Maximum fibre bridging stress, σ_0 (MPa)	Corresponding crack opening, δ_0 (mm)	Strength-based index, σ_0/σ_{fc}	Energy-based index, J'_b/J_{tip}
P2	7.16	0.276	4.16	28.20
P1.75R0.25	6.04	0.247	3.51	23.44
P1.5R0.5	4.79	0.213	2.78	17.81
P1.25R0.75	3.85	0.141	2.24	6.70
P1R1	3.40	0.114	1.97	6.49

3.6. Dynamic compressive behaviour

3.6.1. Failure pattern

The typical dynamic compressive failure patterns of all ECC specimens under different strain rates are illustrated in Fig. 15, indicating that the integrity loss of them went up with the rising strain rate. At a strain rate of 79.6–81.7 s^{-1}, all specimens mostly retained their integrity and only showed some cracks around the edge or splitting cracks across the surface of the loading end. Within this strain rate range, the crack velocity and impact energy were low and the generated cracks had sufficient time to propagate from the edge along the weak zone to the centre area, consuming the impact energy [73]. In the meantime, fibres can effectively restrain the growth of propagating cracks and dissipate the impact energy partly. The impact energy and crack velocity went up as the strain rate increased, generating more cracks to dissipate the energy before the crack propagation through the weak zones [52, 74]. Within a strain rate of 124.1–127.8 s^{-1}, all specimens disintegrated into several fragments with varying sizes. The fibre bridging effect was reduced due to the increased crack size. Most fibres were either pulled out (completely or partly) or ruptured, and fewer fibres bridged the broken fragments. Nevertheless, fibre bridging actions still absorbed a certain amount of energy. Previous studies found a comparable phenomenon for ECC when the strain rate altered [75, 76].

ECC specimens with more PVA fibres tended to have higher impact resistance. For instance, P2 maintained its original shape when the strain rate was within 108.2-110.8 s^{-1}, while ECC specimens containing RTP fibres presented fragmental failure. Even when the strain rate increased to around 124.1-127.8 s^{-1}, several broken fragments were bridged by PVA fibres. Almost no bridging RTP fibres can be identified at the cracking interfaces when the strain rate was higher than 93.6 s^{-1}. However, when the incorporated RTP fibre dosage was appropriate (less than 0.5%), it can create a synergistic effect with PVA fibres to control the cracks that were generated under impact loading. The failure mode of ECC can be also affected by fibre distribution and internal defect distribution [74, 76]. Both longitudinal and transverse cracks can be effectively restrained if most fibres inside

ECC are aligned perpendicular to the loading direction. Given the same reinforcing fibre content, the number of generated micro-cracks under dynamic loading tends to increase with the rising internal defects of ECC.

Mix ID	79.6–81.7 s^{-1}	93.6–96.8 s^{-1}	108.2–110.8 s^{-1}	124.1–127.8 s^{-1}
P2				
P1.75R0.25				
P1.5R0.5				
P1.25R0.75				
P1R1				

Fig. 15. Representative failure patterns of all ECC mixtures after dynamic compression.

3.6.2. Stress-strain response

Fig. 16 displays the stress-strain relationship curves of all ECC specimens, considering a strain rate range of 79.6-127.8 s^{-1}. All curves had a similar shape comprising of two main parts including ascending and descending segments. After impacting the test specimen, the dynamic compressive stress of ECC increased linearly with a small increment of strain, where elastic deformation appeared within this stage. After exceeding the elastic limit, the observed strain increment was caused by the appearance of micro-cracks inside ECC while the micro-cracks propagated slowly because of the fibre bridging actions. During this stage, the compressive stress of ECC followed a non-linear increment trend. Owing to the rapid expansion of initiated cracks, the stress of ECC declined non-linearly up to its ultimate failure. In the meantime, most fibres underwent a sliding or slippage process

before they were completely pulled out or ruptured. No clear residual segments were observed for all studied ECC here. This phenomenon is consistent with other studies [52, 76, 77]. To further quantify the dynamic compressive behaviour of ECC, some essential properties including dynamic compressive strength, peak strain, and energy absorption capacity are discussed as follows.

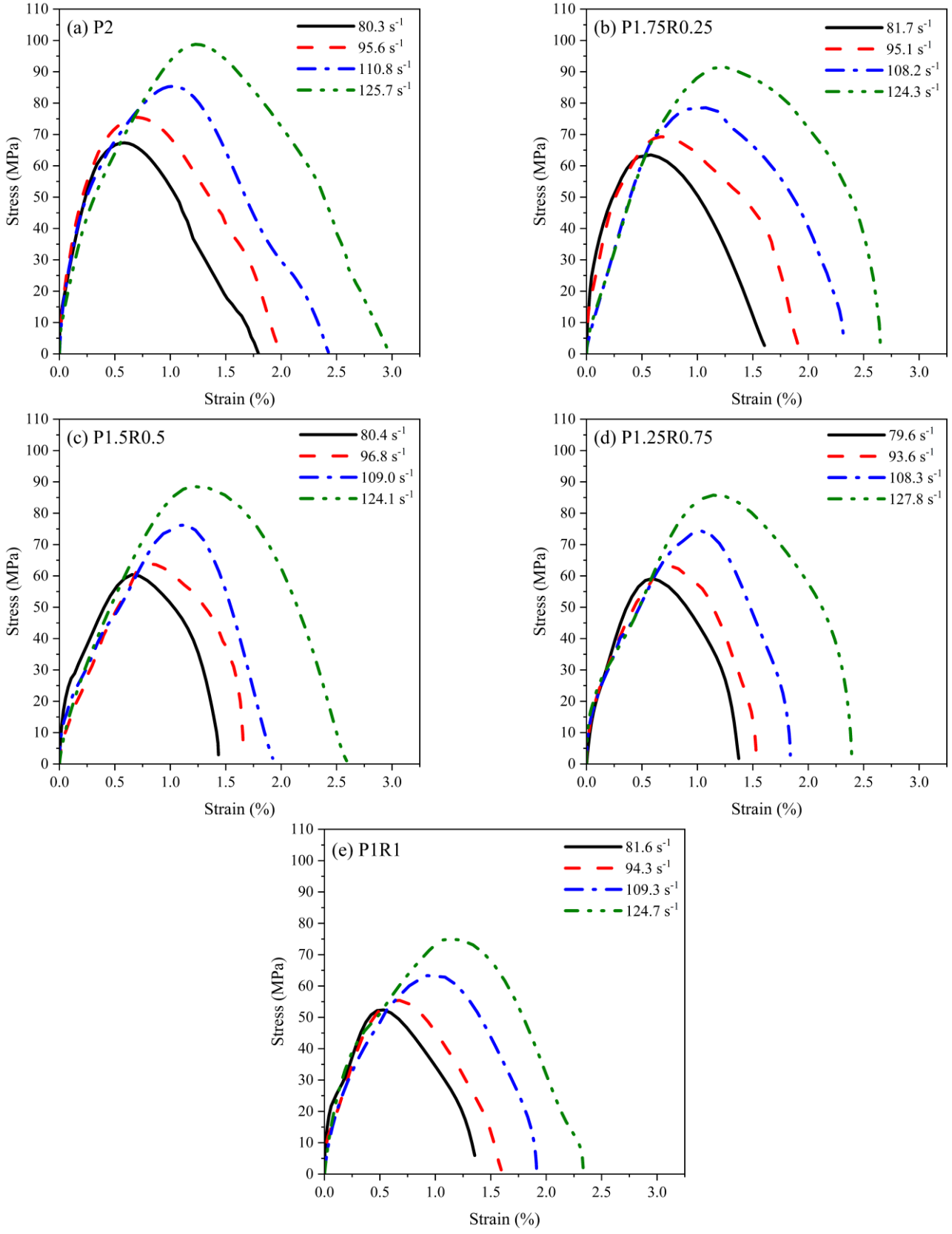

Fig 16. Representative stress-strain curves of all ECC mixtures.

3.6.3. Dynamic compressive strength and energy absorption capacity

Fig. 17 presents the effects of strain rate and fibre on the dynamic compressive strength and energy absorption capacity of ECC, indicating that the dynamic compressive strength of all ECC mixtures was strongly sensitive to the strain rate. For instance, increasing the strain rate led to a 9.14-44.31% improvement in dynamic compressive strength of P1.75R0.25. The strain rate sensitivity can be ascribed to the effects of inertia, time-dependent crack growth and viscosity of free water (Stefan effect) [78-80]. According to Section 2.4.4, all test specimens had an aspect ratio of 0.5, which could diminish the inertia effects whilst the dynamic compression [51, 78]. Thus, the cracking propagation and Stefan effects can be considered as the major factors affecting the strain rate sensitivity of dynamic compressive strength. Following the tendency of dynamic compressive strength, the strain corresponding to the peak stress (peak strain) of all ECC was also enhanced with the rising strain rate. For P2, the peak strain changed from 0.59% to 1.23% when the strain rate increased from 80.3 s^{-1} to 125.7 s^{-1} (Fig. 16). This can be assigned to the reason explained in Section 3.6.1 that increasing the strain rate can result in more micro-cracks inside ECC, which in turn raises the cumulative strain.

At a similar strain rate, the dynamic compressive strength of ECC was lower when the RTP fibre replacement dosage went up. This finding is consistent with other quasi-static properties discussed earlier. At a strain rate of 93.6-96.8 s^{-1}, the dynamic compressive strength of ECC with hybrid PVA and RTP fibres was 8.19-26.56% lower than that of mono-PVA fibre reinforced ECC. This can be attributed to the stronger bridging action provided by PVA fibres under dynamic loading as a result of improved fibre properties and bonding strength. It was reported that the tensile and bond strengths of PVA fibres were enhanced by about 55% and 64%, respectively, when the loading displacement velocity changed from 0.005 mm/s to 50 mm/s [81]. These also can increase the number of pulled out PVA fibres, absorbing more energy and thereby improving the overall strength of composites. Relative to PVA fibres, the properties of RTP fibres after experiencing the strain-rate induced improvement were still insufficient to bridge the macro-cracks, which weakened the crack-controlling ability of ECC when the number of PVA fibres was reduced. However, the difference between ECC with solely PVA fibres and hybrid fibre reinforced ECC in terms of dynamic compressive strength dropped with the rising strain rate, because of the increased possibility of appearing ruptured PVA fibres. When the strain rate was between 124.1 s^{-1} and 127.8 s^{-1}, the dynamic compressive strength of hybrid fibre reinforced ECC was only 7.24-24.03% smaller than that of P2. It was noticed that the chemical bond of PVA fibre reinforced ECC went up considerably with the loading displacement rate [32], which may lead to more ruptured PVA fibres. Considering this drawback of PVA fibre, the presence of RTP fibre is helpful for the properties of ECC under dynamic loading given that the RTP fibre still experienced a pull-out failure under dynamic loading with disparate strain rates [52]. Regarding the peak strain of ECC, varying the fibre dosage did not lead to a noticeable trend (Fig.

16), which is consistent with previous studies that the peak strain was not significantly affected by the presence of fibre [74, 82].

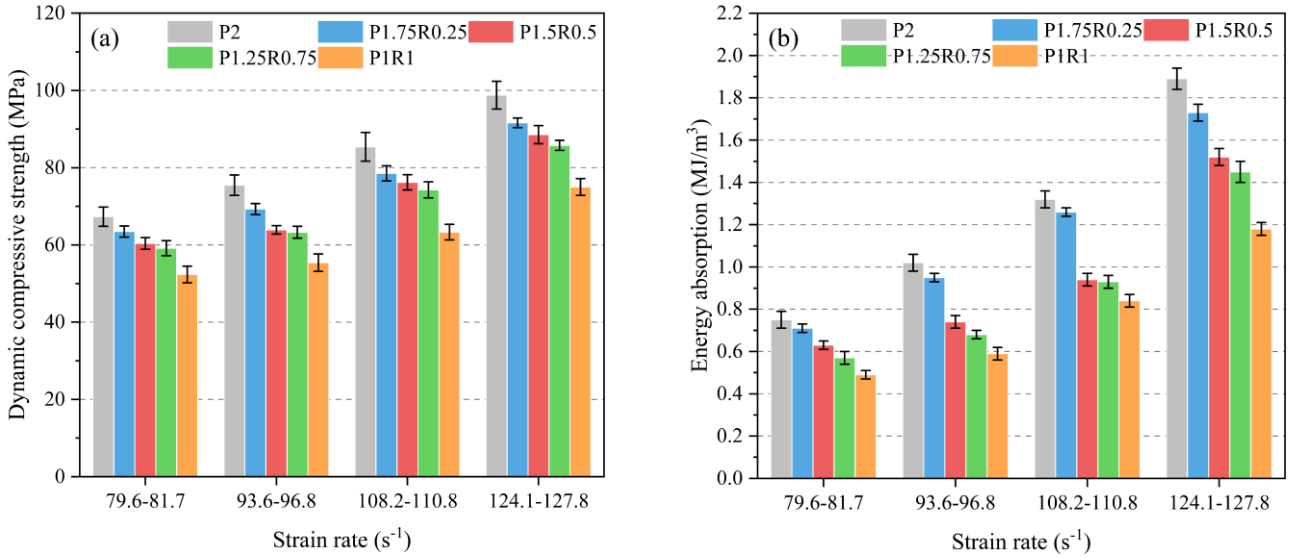

Fig 17. Dynamic compressive properties of ECC: (a) dynamic compressive strength, and (b) energy absorption.

Fig. 17b shows the energy absorption capacity of ECC, which was derived by integrating the dynamic stress-strain curve presented in Fig. 16. Consistent with the dynamic compressive strength and peak strain, ECC absorbed more energy at a higher strain rate primarily because of the generation of more cracks. Different from non-fibre reinforced materials, part of the energy absorbed by ECC was contributed by the fibre bridging effect. Raising the RTP fibre replacement dosage did not benefit the energy absorption capacity of ECC due to the dimension and properties of RTP fibres as well as poorer bonding performance with the matrix. Nevertheless, employing 0.25% RTP fibre to replace PVA fibre in ECC did not substantially diminish its energy absorption capacity as pulled out RTP fibres can partly contribute to improving the energy absorption capacity of ECC. A previous study observed a similar phenomenon that ECC reinforced with both PVA and recycled PET fibres presented an energy absorption of 1.422 J under Charpy impact loading, which was comparable to the mono-fibre reinforced ECC (1.472 J) thanks to the large number of recycled PET fibres experiencing a sliding process during fibre pull-out [11].

3.6.4. Dynamic increase factor

DIF that is the ratio of dynamic compressive strength to quasi-static compressive strength can be used to evaluate the strain rate effect of materials under dynamic loading [83]. Different fitting approaches have been used to describe the relationship between DIF and strain rate [27, 76]. In this study, the linear curve fitting was applied for the DIF versus the logarithm of strain rate and the fitting results are depicted in Fig. 18a and Table 5. The fitted equations of all ECC mixes were reliable as their R^2 were mostly greater than 0.9. Relative to P2, the hybrid fibre reinforced ECC showed higher strain rate sensitivity given their greater gradients of the fitted functions (2.897-3.173). This can be

attributed to the following reasons: (1) the hydrophobic feature of RTP fibres may enhance the Stefan effect as a result of more retained free water [24, 52]; (2) the smaller fibre spacing of RTP fibres can improve the crack-controlling ability of ECC as more RTP fibres are promotive to restraining a single micro-crack; (3) the lower internal quality of ECC with hybrid fibres [84]. It is worth noting that these effects are competing under dynamic loading and the fibre bridging effect is the most dominant one based on the current results. Although hybrid fibre reinforced ECC had a stronger strain rate effect, their dynamic compressive properties were still poorer than those of mono-PVA fibre reinforced ECC owing to the reduced fibre bridging effect.

Table 5 Summary of fitted equations describing the relationship between DIF and strain rate.

Mix ID	Fitted equation	R^2
P2	DIF = $2.780log\dot{\varepsilon} - 4.148$	0.966
P1.75R0.25	DIF = $2.897log\dot{\varepsilon} - 4.389$	0.963
P1.5R0.5	DIF = $3.173log\dot{\varepsilon} - 4.851$	0.900
P1.25R0.75	DIF = $2.964log\dot{\varepsilon} - 4.367$	0.962
P1R1	DIF = $3.000log\dot{\varepsilon} - 4.512$	0.929

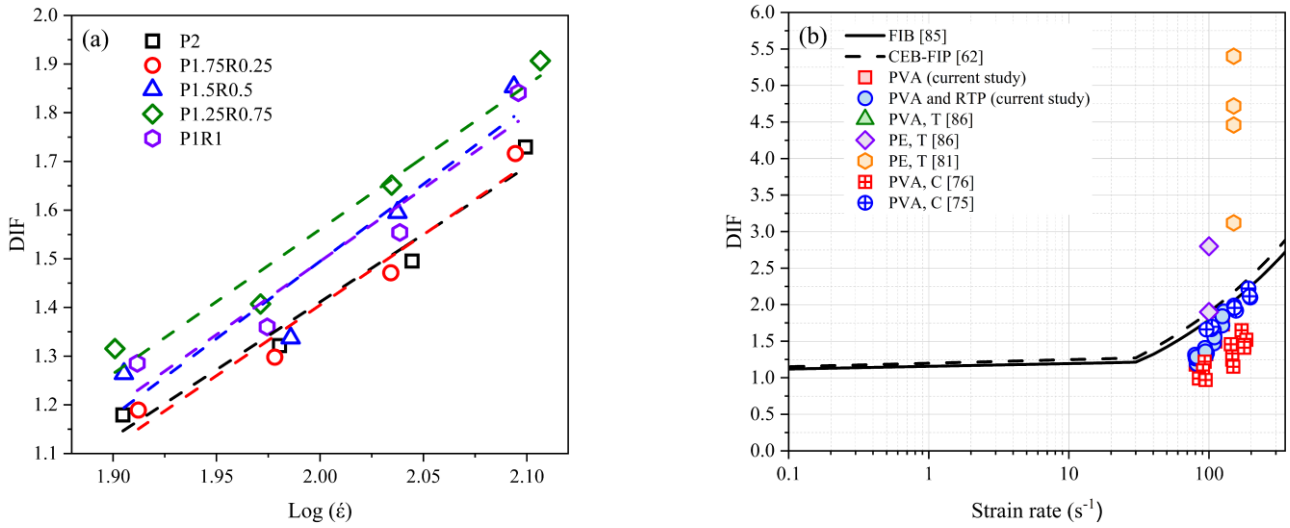

Fig 18. DIF: (a) results of current study, and (b) comparison with existing DIF models and studies (note: T = dynamic tensile DIF, C = dynamic compressive DIF).

The current DIF results were compared with the existing models used for predicting DIF of normal Portland cement concrete [62, 85] and DIF obtained from previous studies on ECC [75, 76, 81, 86] in Fig. 18b. 'T' and 'C' represent the tensile DIF and compressive DIF, respectively. The functions of the used DIF models are presented as follows:

$$DIF_{FIB} = (\frac{\dot{\varepsilon}}{\dot{\varepsilon}_1})^{0.014} \quad for\ \dot{\varepsilon} \leq 30\ s^{-1} \tag{5}$$

$$DIF_{FIB} = 0.012(\frac{\dot{\varepsilon}}{\dot{\varepsilon}_1})^{\frac{1}{3}} \quad for\ \dot{\varepsilon} > 30\ s^{-1} \tag{6}$$

$$DIF_{CEB-FIP} = (\frac{\dot{\varepsilon}}{\dot{\varepsilon}_1})^{1.026\alpha} \quad for\ \dot{\varepsilon} \leq 30\ s^{-1} \tag{7}$$

$$DIF_{CEB-FIP} = \gamma(\frac{\dot{\varepsilon}}{\dot{\varepsilon}_1})^{\frac{1}{3}} \quad for\ \dot{\varepsilon} > 30\ s^{-1} \tag{8}$$

where $\dot{\varepsilon}_1$ = 0.00003 s^{-1}, $\alpha = \frac{1}{(5+9\frac{f_c}{f_{c1}})}$, $\gamma = 10^{(6.156\alpha-2)}$, f_c denotes the quasi-static compressive strength, and f_{c1} = 10 MPa.

The transition strain rate for the above models was 30 s^{-1}, while ECC mixes here seemed to have a larger transition rate, consistent with other ECC specimens in Fig. 18b. All ECC mixtures exhibited lower DIF values than the results predicted by the models at various strain rates. Such discrepancy can be associated with the disparate microstructural and macroscopic performance between normal concrete and ECC. For instance, relative to normal concrete, fewer cracks are induced for ECC due to the effective fibre bridging, which can lower the strain rate sensitivity and thereby smaller DIF. A similar phenomenon was captured for ultra-high performance concrete [79, 82]. At a strain rate of about 150 s^{-1}, the dynamic tensile DIF of PE fibre reinforced ECC ranged from 3.12 to 5.4 [81], which was significantly higher than the dynamic compressive DIF of ECC under a similar strain rate. To ensure a fair comparison between dynamic tensile and compressive DIF, future work should be conducted using the same mix proportion and testing configuration.

3.7. Material cost and sustainability

In this study, embodied carbon and energy were used to indicate the sustainability of ECC [9]. Table 6 lists the material cost, embodied carbon and embodied energy of each mixture, which were calculated based on the market price and life cycle inventory data of each ingredient [87-92]. As expected, the inclusion of RTP fibres lowered the material cost, embodied carbon, and embodied energy of mono-PVA fibre reinforced ECC by 11.13-44.52%, 0.30-1.18%, and 4.47-17.89%, respectively.

Table 6 Material cost and sustainability of ECC mixes.

Mix ID	Material cost (USD/m^3)	Embodied carbon (kg CO_2.eq/m^3)	Embodied energy (MJ/m^3)
P2	886.27	581.17	5533.67
P1.75R0.25	787.63	579.45	5286.23
P1.5R0.5	688.98	577.74	5038.79
P1.25R0.75	590.34	576.02	4791.35
P1R1	491.69	574.31	4543.91

4. Conclusions

In this study, recycled tyre polymer (RTP) fibres were incorporated into polyvinyl alcohol (PVA) fibre reinforced engineered cementitious composites (ECC) for lower material cost and higher sustainability without significantly weakening the engineering properties. A variety of experiments

were carried out to evaluate the effect of RTP fibre replacement level (0.25%, 0.5%, 0.75% and 1.0% by volume) to PVA fibre on the properties of ECC under static and dynamic loadings. Based on the results obtained, the following conclusions can be made:

- The presence of RTP fibres did not benefit the workability, quasi-static compressive strength and elastic modulus of ECC but can improve its drying shrinkage resistance. The drying shrinkage of ECC containing RTP fibres at 28 d was 5-13% lower than that of ECC with 2.0% PVA fibres.
- Although incorporating RTP fibres did not enhance the uniaxial tensile behaviour of ECC primarily due to the poorer fibre bridging stress, all hybrid fibre reinforced ECC fulfilled the requirements for a robust strain-hardening tensile behaviour. Replacing PVA fibres with RTP fibres up to 0.5% can still achieve an acceptable tensile strain capacity (2%) for ECC.
- All investigated ECC mixes were strongly sensitive to strain rate in terms of dynamic compressive properties. ECC with hybrid PVA and RTP fibres exhibited a stronger strain rate effect than ECC with solely PVA fibres. Replacing PVA fibre with 0.25% RTP fibre did not considerably impair the energy absorption capacity of ECC as the large number of RTP fibres experiencing the interfacial sliding process can reimburse the loss of energy induced by ruptured PVA fibres.
- The inclusion of RTP fibres in ECC considerably lowered its material cost and embodied energy, where the estimated benefits were approximately 11-45% and 5-18%, respectively.

Acknowledgements

This research was funded by the National Natural Science Foundation of China (No. 52178382), the Fundamental Research Funds for the Central Universities (No. N2201023) and the Natural Science Funds of Liaoning Province (No. 2020-MS-089). M. Zhang gratefully acknowledges the financial support from the Engineering and Physical Sciences Research Council (EPSRC) under Grant No. EP/R041504/1 and the Royal Society under Award No. IEC\NSFC\191417.

References

[1] V.C. Li, Engineered Cementitious Composites (ECC): Bendable Concrete for Sustainable and Resilient Infrastructure, Springer2019.

[2] V.C. Li, From micromechanics to structural engineering-the design of cementitous composites for civil engineering applications, Journal of Structural Mechanics and Earthquake Engineering 10 (1993) 37-48.

[3] V.C. Li, Engineered cementitious composites (ECC) material, structural, and durability performance, in: E. Nawy (Ed.), Concrete Construction Engineering Handbook, CRC press2008.

[4] J. Qiu, H.S. Tan, E.-H. Yang, Coupled effects of crack width, slag content, and conditioning alkalinity on autogenous healing of engineered cementitious composites, Cement and Concrete Composites 73 (2016) 203-212.

[5] D. Shoji, Z. He, D. Zhang, V.C. Li, The greening of engineered cementitious composites (ECC): A review, Construction and Building Materials 327 (2022) 126701.
[6] H. Zhong, M. Zhang, Engineered geopolymer composites: A state-of-the-art review, Cement and Concrete Composites 135 (2023) 104850.
[7] D. Zhang, J. Yu, H. Wu, B. Jaworska, B.R. Ellis, V.C. Li, Discontinuous micro-fibers as intrinsic reinforcement for ductile Engineered Cementitious Composites (ECC), Composites Part B: Engineering 184 (2020) 107741.
[8] R. Merli, M. Preziosi, A. Acampora, M.C. Lucchetti, E. Petrucci, Recycled fibers in reinforced concrete: A systematic literature review, Journal of Cleaner Production 248 (2019) 119207.
[9] J. Yu, J. Yao, X. Lin, H. Li, J.Y.K. Lam, C.K.Y. Leung, I.M.L. Sham, K. Shih, Tensile performance of sustainable Strain-Hardening Cementitious Composites with hybrid PVA and recycled PET fibers, Cement and Concrete Research 107 (2018) 110-123.
[10] W.-C. Choi, H.-D. Yun, J.-W. Kang, S.-W. Kim, Development of recycled strain-hardening cement-based composite (SHCC) for sustainable infrastructures, Composites Part B: Engineering 43(2) (2012) 627-635.
[11] C. Lu, J. Yu, C.K.Y. Leung, Tensile performance and impact resistance of Strain Hardening Cementitious Composites (SHCC) with recycled fibers, Construction and Building Materials 171 (2018) 566-576.
[12] M.M. Ul Islam, J. Li, R. Roychand, M. Saberian, F. Chen, A comprehensive review on the application of renewable waste tire rubbers and fibers in sustainable concrete, Journal of Cleaner Production 374 (2022) 133998.
[13] Z. Zhang, H. Ma, S. Qian, Investigation on Properties of ECC Incorporating Crumb Rubber of Different Sizes, Journal of Advanced Concrete Technology 13(5) (2015) 241-251.
[14] Y. Wang, Z. Zhang, J. Yu, J. Xiao, Q. Xu, Using Green Supplementary Materials to Achieve More Ductile ECC, 12(6) (2019) 858.
[15] Z. Chen, Y. Liang, Y. Lin, J. Cai, Recycling of waste tire rubber as aggregate in impact-resistant engineered cementitious composites, Construction and Building Materials 359 (2022) 129477.
[16] J. Ye, C. Cui, J. Yu, K. Yu, J. Xiao, Fresh and anisotropic-mechanical properties of 3D printable ultra-high ductile concrete with crumb rubber, Composites Part B: Engineering 211 (2021) 108639.
[17] A. Adesina, S. Das, Performance of engineered cementitious composites incorporating crumb rubber as aggregate, Construction and Building Materials 274 (2021) 122033.
[18] Z. Zhang, F. Qin, H. Ma, L. Xu, Tailoring an impact resistant engineered cementitious composite (ECC) by incorporation of crumb rubber, Construction and Building Materials 262 (2020) 120116.

[19] K. Neocleous, T. Polydorou, K. Pilakoutas, 17 - Reuse of tire constituents in concrete, in: T.M. Letcher, V.L. Shulman, S. Amirkhanian (Eds.), Tire Waste and Recycling, Academic Press2021, pp. 547-564.
[20] A. Baričević, M. Jelčić Rukavina, M. Pezer, N. Štirmer, Influence of recycled tire polymer fibers on concrete properties, Cement and Concrete Composites 91 (2018) 29-41.
[21] M. Chen, Z. Sun, W. Tu, X. Yan, M. Zhang, Behaviour of recycled tyre polymer fibre reinforced concrete at elevated temperatures, Cement and Concrete Composites 124 (2021) 104257.
[22] S.-S. Huang, H. Angelakopoulos, K. Pilakoutas, I. Burgess, Reused tyre polymer fibre for fire-spalling mitigation, Applications of Structural Fire Engineering, 2015.
[23] M. Chen, H. Zhong, L. Chen, Y. Zhang, M. Zhang, Engineering properties and sustainability assessment of recycled fibre reinforced rubberised cementitious composite, Journal of Cleaner Production 278 (2021) 123996.
[24] M. Serdar, A. Baričević, M. Jelčić Rukavina, M. Pezer, D. Bjegović, N. Štirmer, Shrinkage Behaviour of Fibre Reinforced Concrete with Recycled Tyre Polymer Fibres, International Journal of Polymer Science 2015 (2015) 1-9.
[25] A. Baricevic, M. Pezer, M. Jelcic Rukavina, M. Serdar, N. Stirmer, Effect of polymer fibers recycled from waste tires on properties of wet-sprayed concrete, Construction and Building Materials 176 (2018) 135-144.
[26] M. Chen, H. Zhong, M. Zhang, Flexural fatigue behaviour of recycled tyre polymer fibre reinforced concrete, Cement and Concrete Composites 105 (2020) 103441.
[27] M. Chen, W. Chen, H. Zhong, D. Chi, Y. Wang, M. Zhang, Experimental study on dynamic compressive behaviour of recycled tyre polymer fibre reinforced concrete, Cement and Concrete Composites 98 (2019) 95-112.
[28] M. Chen, H. Zhong, H. Wang, M. Zhang, Behaviour of recycled tyre polymer fibre reinforced concrete under dynamic splitting tension, Cement and Concrete Composites 114 (2020) 103764.
[29] H. Zhong, M. Zhang, Dynamic splitting tensile behaviour of engineered geopolymer composites with hybrid polyvinyl alcohol and recycled tyre polymer fibres, Journal of Cleaner Production 379 (2022) 134779.
[30] K.H. Tan, E.H. Yang, S.B. Kang, T.Y. Wahyudi, Mechanical Behaviour of Engineered Cementitious Composites under Quasi-Static and High Strain Rate Applications, Advanced Materials Research 1129 (2015) 10-18.
[31] V. Mechtcherine, O. Millon, M. Butler, K. Thoma, Mechanical behaviour of strain hardening cement-based composites under impact loading, Cement and Concrete Composites 33(1) (2011) 1-11.

[32] E.-H. Yang, V.C. Li, Strain-rate effects on the tensile behavior of strain-hardening cementitious composites, Construction and Building Materials 52 (2014) 96-104.
[33] R. Zhong, F. Zhang, L.H. Poh, S. Wang, H.T.N. Le, M.-H. Zhang, Assessing the effectiveness of UHPFRC, FRHSC and ECC against high velocity projectile impact, Cement and Concrete Composites 120 (2021) 104013.
[34] E.-H. Yang, V.C. Li, Tailoring engineered cementitious composites for impact resistance, Cement and Concrete Research 42(8) (2012) 1066-1071.
[35] GB/T 175-2007, Common Portland Cement, Standards Press of China, Beijing, 2007.
[36] ASTM C618-17a, Standard Specification for Coal Fly Ash and Raw or Calcined Natural Pozzolan for Use in Concrete, ASTM International, West Conshohocken, PA, 2017.
[37] H. Zhong, M. Zhang, Effect of recycled tyre polymer fibre on engineering properties of sustainable strain hardening geopolymer composites, Cement and Concrete Composites 122 (2021) 104167.
[38] O. Onuaguluchi, N. Banthia, Durability performance of polymeric scrap tire fibers and its reinforced cement mortar, Materials and Structures 50 (2017) 158.
[39] ASTM C1437-15, Standard Test Method for Flow of Hydraulic Cement Mortar, ASTM International, West Conshohocken, PA, United States, 2015.
[40] ASTM C490-17, Standard Practice for Use of Apparatus for the Determination of Length Change of Hardened Cement Paste, Mortar, and Concrete, ASTM International, West Conshohocken, PA, United States, 2017.
[41] ASTM C109/C109M-20b, Standard Test Method for Compressive Strength of Hydraulic Cement Mortars (Using 2-in . or [50-mm] Cube Specimens), ASTM International, West Conshohocken, PA, 2020.
[42] ASTM C39/39M-21, Standard Test Method for Compressive Strength of Cylindrical Concrete Specimens, ASTM International, West Conshohocken, PA, United States, 2021.
[43] S. Wang, M.-H. Zhang, S.T. Quek, Effect of Specimen Size on Static Strength and Dynamic Increase Factor of High-Strength Concrete from SHPB Test, J. Test. Eval. 39(5) (2011) 1-10.
[44] J. Xiao, L. Li, L. Shen, C.S. Poon, Compressive behaviour of recycled aggregate concrete under impact loading, Cement and Concrete Research 71 (2015) 46-55.
[45] ASTM C469, Standard Test Method for Static Modulus of Elasticity and Poisson's Ratio of Concrete in Compression, ASTM International, West Conshohocken, PA, United States, 2014.
[46] Japan Society of Civil Engineers, Recommendations for design and construction of high performance fiber reinforced cement composites with multiple fine cracks (HPFRCC), Concrete Engineering Series No. 82 (2008).

[47] K. Yu, Y. Wang, J. Yu, S. Xu, A strain-hardening cementitious composites with the tensile capacity up to 8%, Construction and Building Materials 137 (2017) 410-419.
[48] Y. Wang, H. Zhong, M. Zhang, Experimental study on static and dynamic properties of fly ash-slag based strain hardening geopolymer composites, Cement and Concrete Composites 129 (2022) 104481.
[49] L.-l. Kan, W.-s. Wang, W.-d. Liu, M. Wu, Development and characterization of fly ash based PVA fiber reinforced Engineered Geopolymer Composites incorporating metakaolin, Cement and Concrete Composites 108 (2020) 103521.
[50] RILEM FMC-50, Determination of the fracture energy of mortar and concrete by means of three-point bend tests on notched beams, 18(4) (1985) 287-290.
[51] L.D. Bertholf, C.H. Karnes, Two-dimensional analysis of the split hopkinson pressure bar system, Journal of the Mechanics and Physics of Solids 23(1) (1975) 1-19.
[52] H. Zhong, M. Zhang, Effect of recycled polymer fibre on dynamic compressive behaviour of engineered geopolymer composites, Ceramics International 48(16) (2022) 1151-1168.
[53] W. W. Chen, B. Song, Split Hopkinson (Kolsky) Bar: Design, Testing and Applications, Springer2011.
[54] R. Yu, P. Spiesz, H.J.H. Brouwers, Static properties and impact resistance of a green Ultra-High Performance Hybrid Fibre Reinforced Concrete (UHPHFRC): Experiments and modeling, Construction and Building Materials 68 (2014) 158-171.
[55] N. Ranjbar, M. Zhang, Fiber-reinforced geopolymer composites: A review, Cement and Concrete Composites 107 (2020) 103498.
[56] J. Zhang, C. Gong, Z. Guo, M. Zhang, Engineered cementitious composite with characteristic of low drying shrinkage, Cement and Concrete Research 39(4) (2009) 303-312.
[57] H. Zhu, D. Zhang, Y. Wang, T. Wang, V.C. Li, Development of self-stressing Engineered Cementitious Composites (ECC), Cement and Concrete Composites 118 (2021) 103936.
[58] H. Su, J. Yang, T.-C. Ling, G.S. Ghataora, S. Dirar, Properties of concrete prepared with waste tyre rubber particles of uniform and varying sizes, Journal of Cleaner Production 91 (2015) 288-296.
[59] R. Roychand, R.J. Gravina, Y. Zhuge, X. Ma, O. Youssf, J.E. Mills, A comprehensive review on the mechanical properties of waste tire rubber concrete, Construction and Building Materials 237 (2020) 117651.
[60] K. Yu, Y. Ding, Y.X. Zhang, Size effects on tensile properties and compressive strength of engineered cementitious composites, Cement and Concrete Composites 113 (2020) 103691.
[61] ACI 318, Building Code Requirements for Structural Concrete and Commentary American Concrete Institute, 2008.
[62] CEB-FIP model code 1990: Design code, Comite Euro-Inernational Du Beton 1990.

[63] Z. Zhang, Q. Zhang, Matrix tailoring of Engineered Cementitious Composites (ECC) with non-oil-coated, low tensile strength PVA fiber, Construction and Building Materials 161 (2018) 420-431.
[64] X. Huang, R. Ranade, W. Ni, V.C. Li, On the use of recycled tire rubber to develop low E-modulus ECC for durable concrete repairs, Construction and Building Materials 46 (2013) 134-141.
[65] W.-H. Mao, J.-P. Liu, Y. Ding, High-modulus and low-shrinkage hybrid-fiber reinforced engineered cementitious composites (ECC), Materials and Structures 55(3) (2022) 87.
[66] E. Yang, V.C. Li, Numerical study on steady-state cracking of composites, Composites Science and Technology 67(2) (2007) 151-156.
[67] M. Ohno, V.C. Li, An integrated design method of Engineered Geopolymer Composite, Cement and Concrete Composites 88 (2018) 73-85.
[68] J.-I. Choi, S.-E. Park, Y. Kim, K. Yang, Y.Y. Kim, B.Y. Lee, Highly ductile behavior and sustainability of engineered cementitious composites reinforced by PE based selvage fibers, Cement and Concrete Composites 134 (2022) 104729.
[69] J.-X. Lin, Y. Song, Z.-H. Xie, Y.-C. Guo, B. Yuan, J.-J. Zeng, X. Wei, Static and dynamic mechanical behavior of engineered cementitious composites with PP and PVA fibers, Journal of Building Engineering 29 (2020) 101097.
[70] J. Li, J. Weng, Z. Chen, E.-H. Yang, A generic model to determine crack spacing of short and randomly oriented polymeric fiber-reinforced strain-hardening cementitious composites (SHCC), Cement and Concrete Composites 118 (2021) 103919.
[71] T. Kanda, V.C. Li, Practical design criteria for saturated pseudo strain hardening behavior in ECC, Journal of advanced concrete technology 4(1) (2006) 59-72.
[72] T. Kanda, V.C. Li, Multiple cracking sequence and saturation in fiber reinforced cementitious composites, Concrete Research and Technology 9 (1998) 19-33.
[73] Q. Fu, D. Niu, J. Zhang, D. Huang, M. Hong, Impact response of concrete reinforced with hybrid basalt-polypropylene fibers, Powder Technology 326 (2018) 411-424.
[74] Q. Yu, W. Zhuang, C. Shi, Research progress on the dynamic compressive properties of ultra-high performance concrete under high strain rates, Cement and Concrete Composites 124 (2021) 104258.
[75] M.F. Kai, Y. Xiao, X.L. Shuai, G. Ye, Compressive Behavior of Engineered Cementitious Composites under High Strain-Rate Loading, Journal of Materials in Civil Engineering 29(4) (2017).
[76] Z. Chen, Y. Yang, Y. Yao, Quasi-static and dynamic compressive mechanical properties of engineered cementitious composite incorporating ground granulated blast furnace slag, Materials & Design 44 (2013) 500-508.

[77] B. Zhang, Y. Feng, J. Xie, J. He, Y. Zhang, C. Cai, D. Huang, L. Li, Effects of fibres on ultra-lightweight high strength concrete: Dynamic behaviour and microstructures, Cement and Concrete Composites 128 (2022) 104417.
[78] Y. Hao, H. Hao, G.P. Jiang, Y. Zhou, Experimental confirmation of some factors influencing dynamic concrete compressive strengths in high-speed impact tests, Cement and Concrete Research 52 (2013) 63-70.
[79] J. Lai, W. Sun, Dynamic behaviour and visco-elastic damage model of ultra-high performance cementitious composite, Cement and Concrete Research 39(11) (2009) 1044-1051.
[80] Q. Fu, Z. Zhang, X. Zhao, M. Hong, B. Guo, Q. Yuan, D. Niu, Water saturation effect on the dynamic mechanical behaviour and scaling law effect on the dynamic strength of coral aggregate concrete, Cement and Concrete Composites 120 (2021) 104034.
[81] I. Curosu, V. Mechtcherine, O. Millon, Effect of fiber properties and matrix composition on the tensile behavior of strain-hardening cement-based composites (SHCCs) subject to impact loading, Cement and Concrete Research 82 (2016) 23-35.
[82] G.M. Ren, H. Wu, Q. Fang, J.Z. Liu, Effects of steel fiber content and type on dynamic compressive mechanical properties of UHPCC, Construction and Building Materials 164 (2018) 29-43.
[83] C.A. Ross, J.W. Tedesco, S.T. Kuennen, Effects of strain rate on concrete strength, ACI Mater. J. 92(1) (1995) 37-47.
[84] P.H. Bischoff, S.H. Perry, Compressive behaviour of concrete at high strain rates, Materials and Structures 24(6) (1991) 425-450.
[85] FIB Model Code for Concrete Structures 2010, Comite Euro-Inernational Du Beton 2013.
[86] I. Curosu, V. Mechtcherine, D. Forni, E. Cadoni, Performance of various strain-hardening cement-based composites (SHCC) subject to uniaxial impact tensile loading, Cement and Concrete Research 102 (2017) 16-28.
[87] G. Hammond, C. Jones, F. Lowrie, P. Tse, Inventory of carbon & energy: ICE, Sustainable Energy Research Team, Department of Mechanical Engineering 2008.
[88] Z. Abdollahnejad, F. Pacheco-Torgal, T. Félix, W. Tahri, J. Barroso Aguiar, Mix design, properties and cost analysis of fly ash-based geopolymer foam, Construction and Building Materials 80 (2015) 18-30.
[89] D. Zhang, B. Jaworska, H. Zhu, K. Dahlquist, V.C. Li, Engineered Cementitious Composites (ECC) with limestone calcined clay cement (LC3), Cement and Concrete Composites 114 (2020) 103766.
[90] R. Ranade, Advanced cementitious composite development for resilient and sustainable infrastructure, University of Michigan, 2014.

[91] R. Frazão, R. Fernandes, Comparative Analysis of the Life Cycle of AT Fibre-cement and NT Fibre-cement, International Chrysotile Association (2004).
[92] G.A. Keoleian, A. Kendall, J.E. Dettling, V.M. Smith, R.F. Chandler, M.D. Lepech, V.C. Li, Life cycle modeling of concrete bridge design: Comparison of engineered cementitious composite link slabs and conventional steel expansion joints, J. Infrastruct. Syst. 11 (2005) 51-60.